Heliyon 10 (2024) e38766

Contents lists available at ScienceDirect

Heliyon

journal homepage: www.cell.com/heliyon

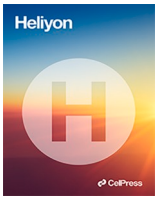

Research article

Effect of microwave sintering on density, microstructural and magnetic properties of pure strontium hexaferrite at low temperatures and heating rate

Wail M. Matran [a], Mazli Mustapha [a,*], Mohd Faizairi Nor [a], Faizal Mustapha [d], Fahd Saeed Alakbari [b,c,**], Gamal Al-shawesh [a], Mohammed Bawahab [e,***]

[a] Department of Mechanical Engineering, Universiti Teknologi PETRONAS, Malaysia
[b] Center of Flow Assurance, Institute of Subsurface Resources, Universiti Teknologi PETRONAS, 32610, Bandar Seri Iskandar, Perak Darul Ridzuan, Malaysia
[c] Centre of Flow Assurance, Institute of Subsurface Resources, Universiti Teknologi PETRONAS, Malaysia
[d] Department of Aerospace Engineering, Universiti Putra Malaysia, Malaysia
[e] Department of Oil and Gas Engineering, Faculty of Earth science, University of Miskolc, Miskolc, Hungary

ARTICLE INFO

Keywords:
Strontium hexaferrites
Ferromagnetic
Magnetic materials
Microwave sintering
Heating rate

ABSTRACT

In recent decades, the rising demand for permanent magnetic materials has driven manufacturers to explore substitutes for rare earth elements in response to their fluctuating prices and negative environmental impact. M-type hexaferrites considered as good alternatives and studies have focused on enhancing their magnetic and structural properties through various approaches. In this study, new approach using low heating rate microwave sintering has been applied to investigate the changes on density, microstructure, and magnetic properties of strontium hexaferrite from core to surface. Sintering temperatures of 950 °C, 1000 °C, 1050 °C, and 1100 °C with 10 °C/minute heating rate were applied accordingly. The bulk density, FESEM, XRD and VSM tests were conducted to study materials' properties. The outcomes of the study showed exponential relationship between density and sintering temperature reaching optimum value of 91.4 % at 1050 °C and then declined slightly at observed to analysis confirmed the magnetoplumbite structure $P6_3/mmc$ in all samples and high crystallized structure at 1050 °C, with the occurrence of α-Fe2O3 at 1100 °C. Grain growth and crystallization observed to increase at higher sintering temperature with agglomeration while denser and melted boundaries at lower temperatures. Magnetic properties especially remanence magnetization Mr and saturation magnetization Ms fluctuated with sintering temperature achieving optimum values of 28.188 emu/g and 55.622 emu/g at 1000 °C respectively. Coercivity Hc and magnetic energy density BH max recorded optimum values at 1050 °C. The findings emphasize the critical role of microwave sintering in tailoring the properties of strontium hexaferrite for magnetic applications.

* Corresponding author.
** Corresponding author. Department of Petroleum Engineering, Universiti Teknologi PETRONAS, Malaysia.
*** Corresponding author.
E-mail addresses: mazli.mustapha@utp.edu.my (M. Mustapha), fahd.akbari@utp.edu.my (F.S. Alakbari), mobawahab@gmail.com (M. Bawahab).

https://doi.org/10.1016/j.heliyon.2024.e38766
Received 17 May 2024; Received in revised form 28 September 2024; Accepted 30 September 2024
Available online 30 September 2024

1. Introduction

The permanent magnetic market has grown significantly, reaching a capital of $21 billion, and is expected to reach $27 billion in 2027 [1]. Rare earth elements (REEs) are known to be used in the manufacturing process of PMs due to their outstanding magnetic performance, high magnetocrystalline and high-energy products [2,3]. Moreover, their ability to facilitate the conversion between motion and electricity enables them to be implemented in many devices that depend on using permanent magnets to operate [4]. China dominates the REEs market, and in the last decade, it raised prices and limited exporting of REEs, causing a fluctuation in the PM market. Considering the ongoing trade tensions between the United States and China and the global COVID-19 pandemic, the situation is on the verge of reaching a critical point [5,6]. Therefore, it is necessary to find competitive substitutions to decrease dependency on REEs. Recently, hexaferrite considered as promising materials studied by PM's development scholars.

Hexagonal ferrites typically comprise six elements, indicated as M, Z, Y, W, X, and U. M-type hexaferrites with the chemical formula $MFe_{12}O_{19}$ (M = Ba, Sr, Pb, and Ca) have gained attention from numerous researchers and industries due to their good magnetic and physical properties, including a high Curie temperature (450 °C), large magnetocrystalline anisotropy, high magnetization, low dielectric loss, high chemical stability, high resistivity, high coercive field, and good corrosion resistance. In addition, easy mass production, fabrication, low cost, and low environmental consequences compared to REEs make them promising materials for hard magnetic applications such as recording media drives, microwave devices, radar-absorbing materials, and wireless communications [2,4,7,8].

Researchers have applied different methods to enhance the magnetic properties and microstructure of hexaferrites. Starting from synthesizing, advanced synthesis processes have shown better microstructure and magnetic coercivity than conventional processes by producing small grain size and pure components [9–11]. Some studies have reported sol-gel, co-precipitation, and auto-combustion sol-gels effective methods to process hexaferrite powders, although conventional methods attain cost and simplicity advantages [9, 12–14]. Ion substitution and additives are also reported to tune the properties of hexaferrite during the synthesis or sintering process by either improving magnetic properties and microstructure or lowering the calcination temperature [2,13,15]. One of the crucial procedures in the processing and manufacturing of hexaferrite ceramics is sintering. The sintering process can be affected by the heating rate, temperature, pressure, and atmosphere [16–18]. Moreover, it is responsible for solidification and microstructure changes such as grain growth and reducing voids' size and content [19].

Hexaferrite magnets are currently produced using conventional sintering methods due to their simplicity and low cost [20]. However, conventional methods are inefficient in saving energy due to the dissipation of heat to the surroundings and require more time to reach the desired temperatures. Therefore, researchers have developed modern sintering techniques that enable low-temperature sintering, consume less time, and save energy [20–23]. In these studies, radiative heating as in microwave sintering (MS) [17,24], high pressure and electrical current as in splash plasma sintering (SPS) [25–27], and solvents as in cold sintering are utilized [28,29]. Microwave sintering is more practical on a large scale than SPS, while cold sintering has a limited production scale and requires complex equipment [29,30]. Furthermore, microwave sintering offers several advantages, including the ability to selectively heat materials from the core to the surface using high-frequency electromagnetic waves, achieving uniform heating, rapidly adjusting temperatures, operating at lower process temperatures, and reducing sintering time compared to traditional sintering methods [20,21,31,32].

It is noted that the existing literature on the microwave heating mechanism's influence on the microstructure and magnetic properties development of strontium hexaferrite is limited. First work studied microwave sintering effects on strontium hexaferrite was done in 1999, and it reported 87.3 %–87.0 % relative density at 1065 °C and 1075 °C respectively [24]. Other study done in 2013, produced strontium hexaferrite using microwave sintering method reported a magneto plumbite phase in XRD and value of 50.43 emu/g and coercivity higher than 2 KOe at 1150 °C sintering temperature and 50 °C/min heating rate [33]. In 2013, C. Z. Yan et al., have also conducted MS at a high-temperature heating rate of 30 °C/min and compared it to conventional method in which pure SrM produced at lower sintering temperature using microwave method [23], while others have conducted MS in strontium ferrite with one or more additive materials such as barium, and REEs [34–36]. Only one work conducted in 2009 studied microwave sintering effects on barium hexaferrite at low heating rate of 8 °C/minute and sintering temperature of 840 °C which produced Ms of 53.6 emu/g and coercive force 623.8 Oe [23]. No research has yet demonstrated the effects of microwave sintering (MS) under low heating rate conditions on pure strontium ferrite ceramic, nor has it explored the microwave heating effect from core to surface perspectives. Therefore, it is crucial to study the effects of a low heating rate on strontium ferrite using advanced sintering methods. In this respect, the objective of the present work was to study the influence of microwave sintering at low heating rate conditions of different sintering temperatures on microstructure development and magnetic properties of pure strontium hexaferrite ceramic.

2. Experimental methods

2.1. Materials

Nanocrystallites of M-type strontium hexaferrite ($SrFe_{12}O_{19}$) powder with 0.045 mm average particle size, (99.5 % purity) and weighing 25 g, was purchased from (Sigma-Aldrich (M) Sdn Bhd, Selangor D.E, Malaysia), and used as a starting material for this study.

2.2. Methodology

Strontium hexaferrite powder was separated into samples for green compaction process. Each sample has a weight of 3 ± 0.5 g. A

hollow cylindrical steel die was used with dimensions of 12 ± 0.5 mm inner diameter and 7 ± 0.5 mm height. The green compaction was performed using a hydraulic shop press machine with a 20 tons limit. A pressure of 5 tons was applied to all samples, as recommended in Ref. [37] using upper and lower punches to create uniaxial pressure. Using a calibrating tool, the compacted samples were then placed on a cylindrical-shaped alumina substrate in the furnace heating room. The sintering process took place in an HAMiLab-V3000 microwave furnace (University Malaysia Perlis, Perlis, Malaysia) with a frequency of 2.45 GHz and a power range of 0.5–2.85 kW. Sintering conditions included a micro vacuum of 0.025 kPa, a heating rate of 10 °C/min, and varied sintering temperatures at 950 °C, 1000 °C, 1050 °C, and 1100 °C which are considered as 80 to 90 percent of melting point of the material. In addition, a 1-h holding time, as recommended in the literatures [27,38]. The samples were cooled normally without any forced cooling by slow cooling to room temperature [16].

2.3. Characterization

The bulk density of the sintered samples was estimated using the Archimedes method. Afterward, the samples were dried in an oven at 70 °C for 1 h. Vertical cuts were made from the center of the samples to study core and surface microstructure. Mounting, grinding, and polishing processes were performed using Simplimet 1000 and Metaserv 2000, respectively, to prepare sintered materials for further analysis. X-ray diffraction analysis (XRD) with Cu-Kα radiation ($\lambda = 1.5406$ Å) was conducted in the centralized analytical laboratory (CAL-UTP-Perak-Malaysia) to record the crystal structure of the sintered ferrite samples at room temperature. X'pert HighScore and Origin software were used to refine and examine the XRD patterns in the angular range $20° \leq 2\theta \leq 80°$ to identify the structural phases of the samples. Field emission scanning electron microscopy (FESEM), EDX and mapping using SUPRA 55VP by Carl Zeiss AG in the centralized analytical laboratory (CAL-UTP-Perak-Malaysia) were employed to enhance the understanding of the samples by investigating their microstructure, morphology, and studying the distribution of elements. Moreover, linear intercept method has been employed to measure average grain size of the sintered SrM. Hysteresis loop measurements at room temperature were used to analyse the magnetic properties of the powdered samples with different sintering temperatures. This was done employing vibrating sample magnetometry (VSM) with a Lakeshore VSM 7400 at Nanocat University of Malaya, Kuala Lumpur, Malaysia. The instrument operated under an applied magnetic field ranging up to ±8 kOe.

3. Results and discussion

3.1. Density analysis

The effect of sintering temperature on the density of strontium hexaferrite is presented in Table 1. At a low sintering temperature of 950 °C, strontium hexaferrite exhibited low density and a relative density of 87.83 %, which is the lowest in this research. The relative density of strontium hard magnetic then increased, reaching 89.76 % at 1000 °C. At 1050 °C, the density of the strontium ferrite reached its optimum value of 4.7366 g/cm3, with a relative density of 91.44 % (5.18 g/cm3) as reported in Ref. [39]. In comparison to the density at 1050 °C, the density value at 1100 °C sintering temperature inclined, reaching a value of 4.6246 g/cm3 and a relative density of 89.28 %, which is lower than the sample sintered at 1000 °C. The change in density with different sintering temperatures can be an effect of grain growth, densification, defects existence, and impurities. Further investigation of the crystal structure and morphology of SrFe12O19 can answer the behaviour of density at different sintering temperatures. In this work, relative density of 91.44 % have been achieved which is higher than study used plasma sintering method which recorded optimum relative density of 85 % [40]. Moreover, other study used microwave reported optimum relative density of 87 % which lower than current study [24]. Other studies used conventional sintering method and cold sintering method reported relative densities of 90 % using cold sintering [28]. Only study that used microwave sintering at lower heating rate on BrM achieved relative density of 97.5 % which is the highest among all studies [37].

3.2. XRD analysis

The X-ray diffraction phase analysis conducted on all strontium hexaferrite samples, regardless of the sintering temperatures, at micro vacuum in the angular range $20° \leq 2\theta \leq 80°$, revealed a match between patterns of all sintered samples and SrFe12O19 in JCPDS reference number 33–1340 as shown in Fig. 1. A single magnetoplumbite structure ($P6_3/mmc$) can be observed in all samples. Strontium samples sintered at 950 °C, 1000 °C, and 1050 °C did not reveal an obvious secondary phase, while sample sintered at 1100 °C showed a small diffraction of α-Fe2O3 co-existing with the strontium hexaferrite phase, which was reported in many studies [28,41,42]. This phase presence indicates that strontium ferrite is not fully crystallized at 1100 °C, although similar peaks of α-Fe2O3 were detected in the reference patterns.

The sample sintered at 1050 °C exhibited higher intensity and peaks number, followed by the sample sintered at 1100 °C, compared

Table 1
Density and relative density of strontium ferrite sintered at 950 °C, 1000 °C, 1050 °C, and 1100 °C.

Sintering temperature	950 °C	1000 °C	1050 °C	1100 °C
Density (g/cm^3)	4.5498	4.6477	4.7366	4.6246
Relative Density (%)	87.83	89.76	91.44	89.28

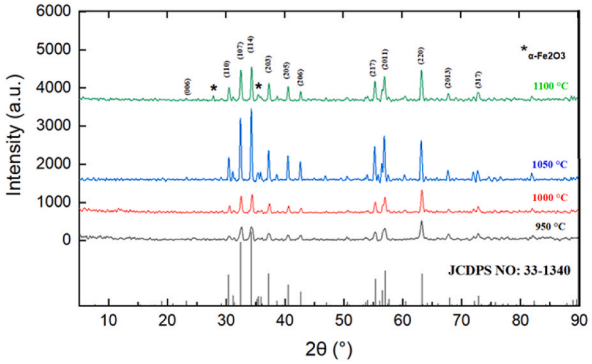

Fig. 1. Typical XRD patterns and peaks (hkl) of SrFe12O19 sintered at different temperatures compared to reference pattern.

to samples sintered at 950 °C and 1000 °C, which showed less crystallized patterns. The sharp peaks and higher intensity of strontium ferrite sintered at 1050 °C resulted in denser material, as shown in Table 1, which is a result of the highly crystallized structure. The decline in the density of the sample sintered at 1100 °C compared to the sample sintered at 1000 °C can be related to the existence of the hematite phase in multiple points, although it showed a better crystalline structure. This decline can be related to the presence of hematite, higher multistage boundary melting, and consolidation caused by high-temperature sintering. Several studies have reported similar XRD pattern of strontium hexaferrite sintered using different methods and sintering temperatures including [43–45]. Moreover, studies revealed a detection of second phase of strontium and impurities in their sintered samples at different temperatures such as 1250 °C [43], 1100 °C [46], 1000 °C [44].

Fig. 2 shows the XRD pattern of sintered samples compared to two reference patterns of ICDD. Reference number 96-100-8856 has the most matches to the sample's pattern compared to reference number 96-152-7076. Both references are SrFe12O19 and have a magnetoplumbite structure. Matches between reference number 96-100-8856 and the sample sintered at 1050 °C are mostly identical and contain rich peaks' numbers and intensity, while other samples exhibited lower peaks and intensity. Samples shared peaks with hkl numbers (110), (107), (114), (203), (205), (217), (2011), (220), and (317). According to Figs. 1 and 2, the (114) peak of the samples showed a low-scale shift, and it maintained a position closer to the main reference than the other reference. Similar peaks and structure

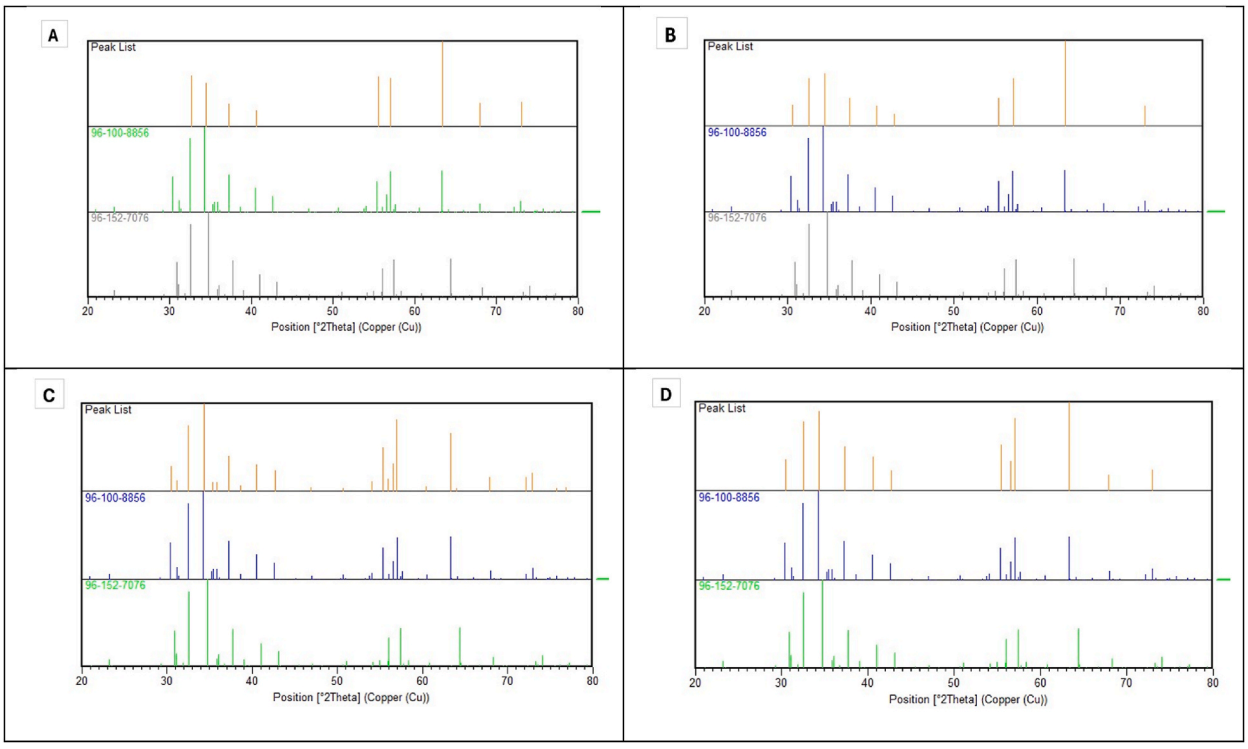

Fig. 2. XRD pattern of samples sintered at 950 °C (A), 1000 °C (B), 1050 °C (C), and 1100 °C (D) compared to ICDD reference no 96-100-8856 (middle) and references no 96-152-7076 (bottom).

have been observed in study that strontium crystal structure [47]. The growth of peak (006) intensity in samples sintered at 1050 °C and 1100 °C confirms that the orientation of the growth of SrFe12O19 is along the c-axis, as revealed in Ref. [27].

Texture coefficient (TC) values of sintered strontium hexaferrite from XRD results have been calculated using equation (1).

$$TC_{(hkl)} = \frac{I_{(hkl)}/I_{0(hkl)}}{\left(\frac{1}{N}\right)\left[\sum_N \frac{I_{(hkl)}}{I_{0(hkl)}}\right]} \quad (1)$$

Where, I0 (hkl) and I (hkl) correspond to the standard and the determined relative intensities of the single crystal plans (hkl), and N represents the peak number. In this equation, the peak intensities of the sintered sample are computed and compared to those of the matched reference code. The enhancement in the (00l) peak intensity on the top surface of the magnetically aligned sample suggests a better c-axis orientation. Consequently, the peak intensity for peaks (006), (008), (107), (114), (2011), and (220) in the sintered samples influenced by the external magnetic field appeared notably higher compared to other peaks. This indicates a more noticeable grain orientation along these crystallographic directions. Therefore, the Texture Coefficient (TC) can be employed as a qualitative measure to ascertain the grain's orientation if it's around easy magnetization c-axis or another axis such as hard magnetization b-axis [48].

Table 2 illustrates a trend where sample sintered at 950 °C exhibited a decreased Texture Coefficient (TC) values for planes (006), (008), (107), and (114), registering TC values of 0.61, 0.47, 0.305, and 0.354, respectively. Conversely, planes (220) and (2014) display the highest TC values, indicating a prevalent orientation of grains along the hard magnetization b-axis rather than the c-axis. This deviation from c-axis preference can be attributed to the insufficient sintering temperature, preventing atoms from aligning around the easy magnetization axis. TC values for planes (006), (008), (107), and (114) remain relatively low compared to (2011), (220), and (2014), indicating a weak preference for c-axis orientation despite increased sintering temperature to 1000 °C. This suggests a dynamic reorientation of grains between easy and hard axes. Furthermore, Table 2 highlights significantly high TC values for planes along the c-axis, notably for (006), (008), (107), and (114), suggesting predominant growth along the easy magnetization axis due to increased sintering temperature to 1050 °C, enhancing grain orientation and intensity. Conversely, samples sintered at 1100 °C exhibit improved orientation and TC values for planes (006), (008), (107), and (114) compared to those sintered at 950 °C and 1000 °C. Although all c-axis planes display relatively high TC values, indicating marginal growth along the easy magnetization axis compared to the hard axis, the TC values for planes (220) and (2014) are notably higher, potentially influenced by secondary phase formation due to thermal decomposition of SrFe12O19 at higher sintering temperatures.

To investigate change in average crystalline size (ACS) and strain in pure strontium hexaferrite sintered at different temperatures, Scherer equation (2) and W-H equation (3) and plot utilized accordingly.

$$D = K\,\lambda\,/\,\beta\cos\theta \quad (2)$$

$$\beta\cos\theta = K\,\lambda\,/D + 4\,\epsilon\,\text{sine}\,\theta \quad (3)$$

Where D is the crystallite size, K is a dimensionless shape factor (typically around 0.9), λ is the X-ray wavelength, β is the FWHM of the diffraction peak, θ is the Bragg angle and ϵ is the lattice strain.

The result can be seen in Table 3. It can be observed that the crystalline size increased as ST increased from 950 °C to 1050 °C. However, its notable by increasing sintering temperature to 1100 °C the crystalline size decreased. Sample sintered at 1050 °C recorded an ACS value of 63.212 nm which is the optimum overall. The decrease in ACS in sample sintered at 1100 °C due to formation of other phases and cavity appearance.

Microstrain value of sintered samples can be shown in Table 3. All samples exhibited compression and shrinkage in their microstrain except sample sintered at 1050 °C which recorded a positive value of 0.000788 while samples sintered at 950 °C, 1000 °C and 1100 °C recorded a negative value of 0.0018, 0.00048, and 0.0028 respectively.

Fig. 3(A–D) presents the W-H plot of microstrain where slope line of all sintered sample is declining except sample sintered at 1050 °C that attains rising slope line which is due to higher point recorded. The shrinkage in samples can be due to phase transformation and internal stresses from compression process of the samples [49]. Moreover, anisotropy preferred orientation can be shown in sample

Table 2
The calculated TC of sample sintered at 950 °C, 1000 °C, 1050 °C, and 1100 °C.

	Crystal planes						
Plane	(006)	(110)	(008)	(107)	(114)	(203)	(205)
TC (950 °C)	0.61	0.246	0.47	0.305	0.354	0.417	0.4685
TC (1000 °C)	0.28	0.31	0.336	0.33	0.347	0.546	0.6
TC (1050 °C)	0.97	1.36	1.46	1.86	1.85	1.74	2.15
TC (1100 °C)	0.837	0.768	0.65	0.8	0.82	1.00	1.255
Crystal planes							
Plane	(206)	(217)	(0014)	(2011)	(220)	(2014)	(317)
TC (950 °C)	0.7	0.61	0.188	0.655	1.05	1.58	0.785
TC (1000 °C)	0.62	0.71	0.23	0.84	1.22	0.8	0.66
TC (1050 °C)	2.47	2.35	2.0	2.4	2.07	2.08	1.47
TC (1100 °C)	1.23	1.38	0.48	1.3	1.62	1.6	0.64

Table 3
ACS and microstrain of sintered strontium samples.

Sample	Average Crystalline Size (nm)	Microstrain
(A) 950 °C	24.522	−0.00118
(B) 1000 °C	38.437	−0.00048
(C) 1050 °C	63.212	0.000788
(D) 1100 °C	47.244	−0.00028

sintered at 1050 °C which resulted in tensile strain and higher value single point.

3.3. FESEM analysis

Fig. 4 illustrates the FE-SEM patterns of strontium hexaferrite sintered at 950 °C, 1000 °C, 1050 °C, and 1100 °C. It can be observed that grain growth and crystallization increased with the rising of sintering temperature. The grain size transitioned from fine to coarse grains as the sintering temperature increased. The sample sintered at 950 °C revealed a denser image with high melting boundaries and fewer voids, although it exhibited the lowest density value among all samples. The grain growth and interconnection were not as apparent at this sintering temperature. At 1000 °C sintering temperature, strontium ferrite exhibited behaviour similar to the previous sintering temperature, showcasing a denser image, high melting boundaries, and fine grains. However, small defects and voids were observed in this sample compared to the sample sintered at a lower temperature. The grain sizes at 950 °C and 1000 °C ranged from less than 0.2 μm to more than 10 μm. On the other hand, samples sintered at 1050 °C and 1100 °C revealed high grain growth and well-crystallized, coarse grains. Agglomeration was noted in these samples, and it was higher than in the other two samples sintered at lower temperatures. Grain sizes in these two samples ranged from 0.5 μm to more than 20 μm. The core view of the sample sintered at 1100 °C showed denser and finer grains compared to the surface view with sharp shapes. In terms of previous studies, 1.2–9 μm average grain size (AGS) has been reported using conventional sintering 28 [50] and (AGS) 5–10 μm has been recorded using microwave method which close to conventional method and current study result [37]. Moreover, 0.5–2 μm AGS has achieved using cold sintering [51]. Almost similar voids and boundaries are reported in many studies, including [37,50], and [51], which make the microstructural outcomes of this work consistent with previously observed phenomena.

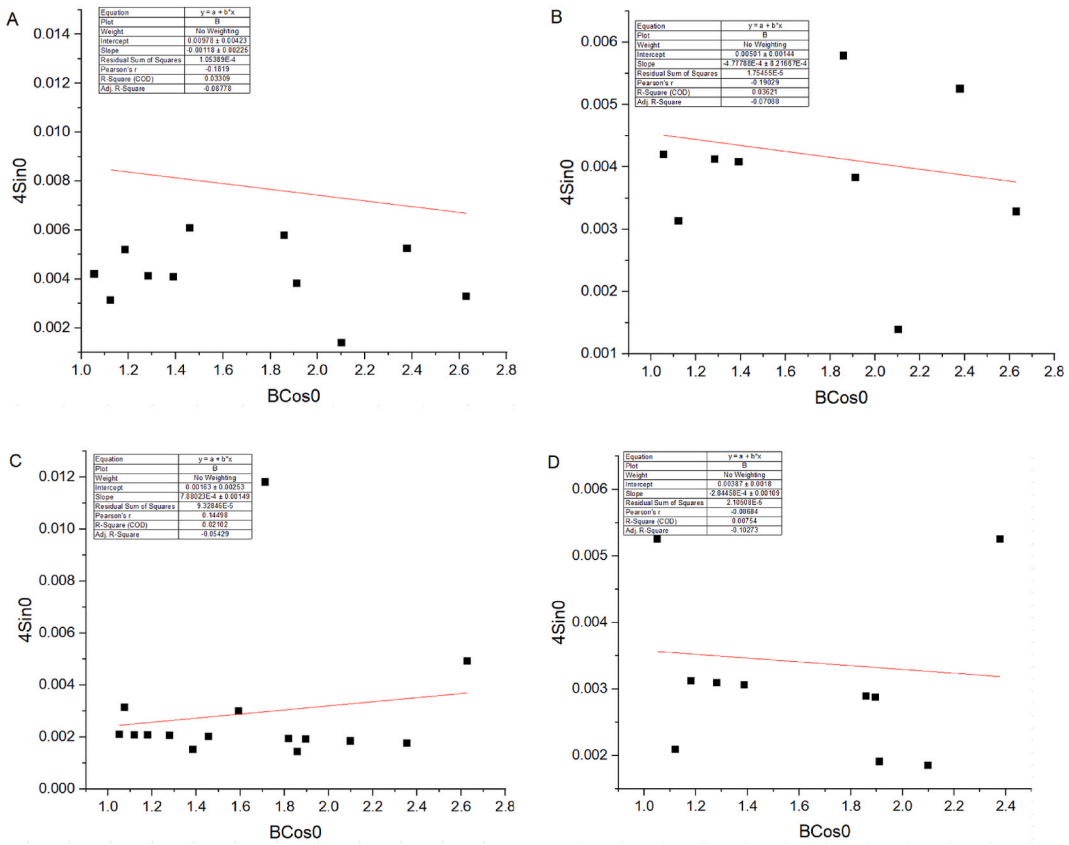

Figure 3. W-H plot of microstrain of samples sintered at 950 °C (A), 1000 °C (B), 1050 °C (C), and 1100 °C (D).

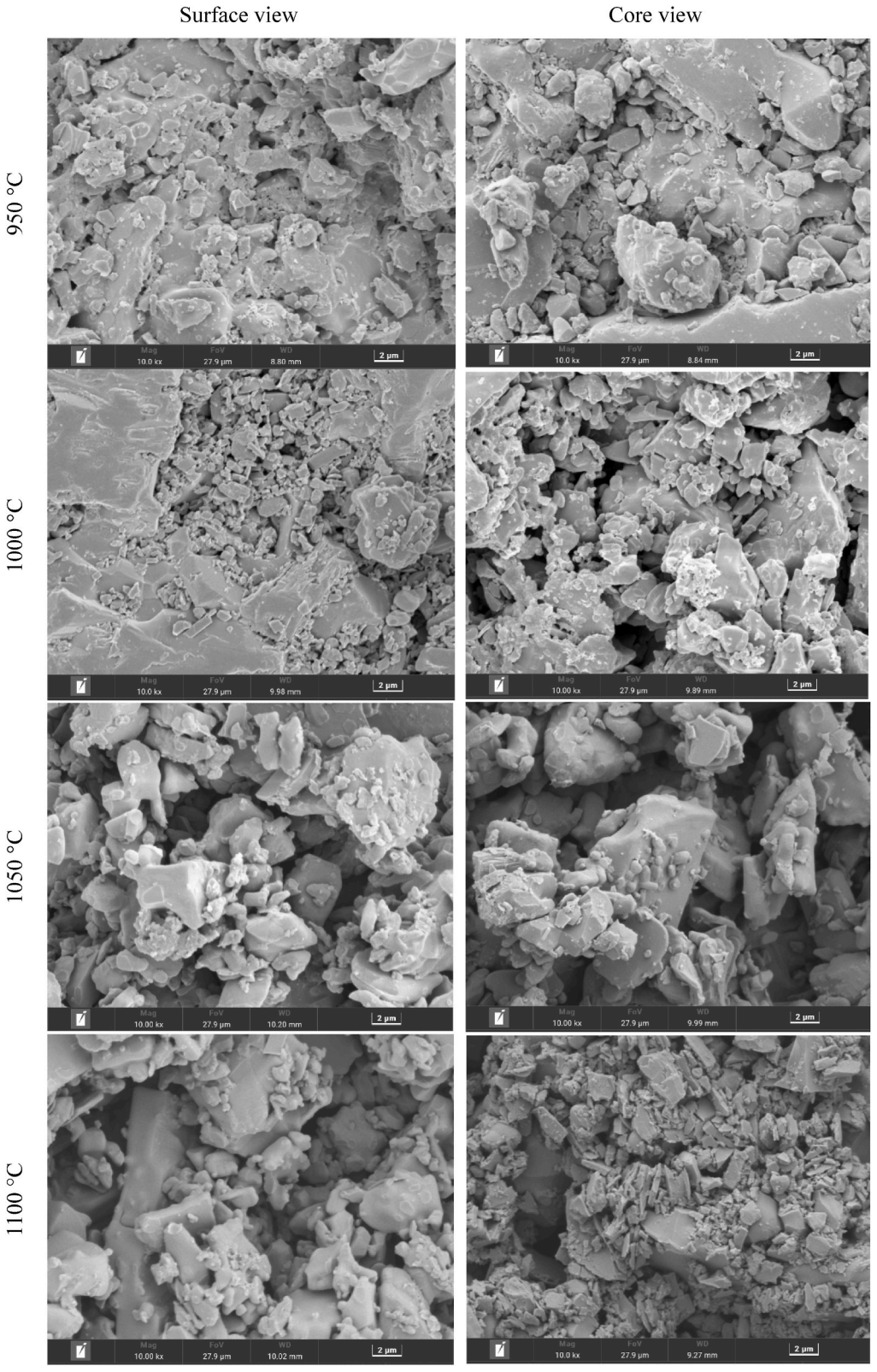

Fig. 4. Microstructural evolution of strontium ferrite ceramic samples sintered at 950 °C 1000 °C 1050 °C 1100 °C various temperatures.

To investigate the elemental distribution of sintered strontium ferrites, EDX values, spectra and mapping were performed, as shown in Table 4, Figs. 5 and 6(a and b) respectively. In the general view, there was a homogeneous distribution of Fe and O elements in all samples. Carbon distribution was higher on the surface of the samples sintered at 950 °C and 1000 °C, while samples sintered at 1050 °C and 1100 °C exhibited higher carbon distribution in the core, as shown in Figs. 5 and 6 (a,b). Table 4 presents the wt.% of elements at different sintering temperatures of sintered strontium ferrite according to surface and core regions. On the surface, the wt.% of all elements were mostly close, except for the sample sintered at 950 °C, which showed a higher wt.% of carbon and a lower wt.% of Fe. The values of carbon and Fe elements in the sample sintered at 950 °C were 17.6 % and 58.6 %, respectively, which may explain the dense surface and melting boundaries of this sample in the SEM view. The higher carbon percent initiated from the sintering furnace where carbon is produced from the burning process in the microwave furnace. The sample sintered at 1050 °C showed a higher percent of Fe with a value of 71.0 % on the surface, which explains the higher density of this sample compared to the sample sintered at 950 °C, which showed the lowest density and Fe percentage. The distribution of elements in the core is mostly close. The sample sintered at 1000 °C obtained a higher wt.% of iron with 70.5 % compared to the sample sintered at 1100 °C, which obtained 65.1 %, which may be the reason for the lower density of this sample since iron density (7.874 g/cm^3) is the highest compared to Sr (2.64 g/cm^3), O (gas), and C (2.25 g/cm^3) and strontium hexaferrite is a compound contains one strontium atom, 12 iron atoms and 19 oxygen atoms.

3.4. VSM analysis

Fig. 7 shows the (M/H) hysteresis loop of the sintered SFO at different temperatures. The hysteresis curves of samples represent attributes of ferromagnetic materials, and samples sintered at 1000 °C and 1050 °C showed smoother and wider curves compared to the other two samples, confirming hard magnetic behavior. The effects of different sintering temperatures at low heating rates on the magnetic properties of strontium hexaferrite are shown in Table 5. The values of magnetic properties of sintered samples varied according to the temperature and BHmax value is magnetic energy resulted from coercivity field (Oe) multiplied with magnetization saturation Ms (emu/g). Therefore, any change in coercivity and magnetization saturation can affect BHmax values. Coercivity and magnetization are affected from sintering temperature, grain size, and impurities in the material such as hematite. The magnetization remanence (Mr) value increased with increasing sintering temperature, reaching an optimum value of 28.188 emu/g at 1000 °C, and then decreased to the lowest value of 23.691 emu/g at 1100 °C. The saturation magnetization value (Ms) fluctuated with sintering temperature, initially increasing from 950 °C to 1000 °C, achieving an optimum value of 55.622 emu/g, decreasing to 54.451 emu/g at 1050 °C which is less by 2.105 percent of the overall optimum value, and finally increasing to 54.719 emu/g at 1100 °C which can be effect of hematite phase existence. On the other side, coercivity and (BH)max increased with increasing sintering temperature, recording an optimum coercivity value of (BH)max of 34068.17 emu.Oe/g and 1252 Oe at 1050 °C which is higher by 35.37 % compared to value recorded in sample sintered at 1000 °C. At 1100 °C, coercivity and (BH)max decreased significantly, recording 858.28 Hc and 20333.51 (BH)max. Samples sintered at 1000 °C and 1050 °C showed optimum magnetic properties due to their high density, high phase purity, well-defined crystallinity, and good magnetic lattice.

In terms of coercivity, samples that exhibited higher values showed better grain shapes, sizes, and structure, especially in the core view as study revealed [33]. The sample sintered at 1100 °C recorded the lowest values, and this could be due to the presence of hematite in the material, internal strain, and morphological changes as seen in Fig. 4 [52,53]. While the sample sintered at 950 °C showed moderate records with reasonable magnetic values. The squareness ratio of Mr/Ms as shown in Table 5 differentiates materials according to the value, where a value less than 0.4 and reaching zero indicates particle interaction by magneto-static interaction and attains domain-wall formation. While materials that have Mr/Ms values about 0.4 and larger obtain the ideal Stoner-Wohlfarth value and single domain for randomly oriented uniaxial grains according to Ref. [54] considering them as hard magnetic materials. Samples in this study recorded Mr/Ms values over 0.4, and the optimum values were 0.507 and 0.5 at 1000 °C and 1050 °C, respectively. In comparison to other studies, the magnetic values of Ms, Mr, and Hc achieved in this study is better than reported values reported in the stdy that employed low heating rate microwave sintering [24]. Moreover, this work showed magnetic properties better than many works, thus several studies reported higher values using high heating rate and sintering method which can be seen in Table 6. Coercivity values of all samples recorded higher values than 0.125 kOe, which is the minimum value for hard magnetic material to be used in applications such as recording media, headphones, and antennas [54–56].

4. Conclusion

In conclusion, the impact of microwave sintering at low temperature heat rate on strontium hexaferrite has been systematically examined. At lower sintering temperatures, such as 950 °C, the material exhibited a lower relative density of 87.83 %, indicating less

Table 4
EDX percentage of elemental distribution of sintered strontium ferrite (SrFe12O19) at different temperatures.

	Surface (wt.%)				Core (wt.%)			
	Fe	O	Sr	C	Fe	O	Sr	C
950 °C	58.6	18.1	5.7	17.6	70.2	15.8	5.8	8.2
1000 °C	66.5	18.4	6.3	8.7	70.5	15.4	5.2	8.8
1050 °C	71.0	15.3	5.8	7.9	67.4	17.4	6.0	9.2
1100 °C	69.4	17.1	6.1	7.4	65.1	19.1	6.9	8.8

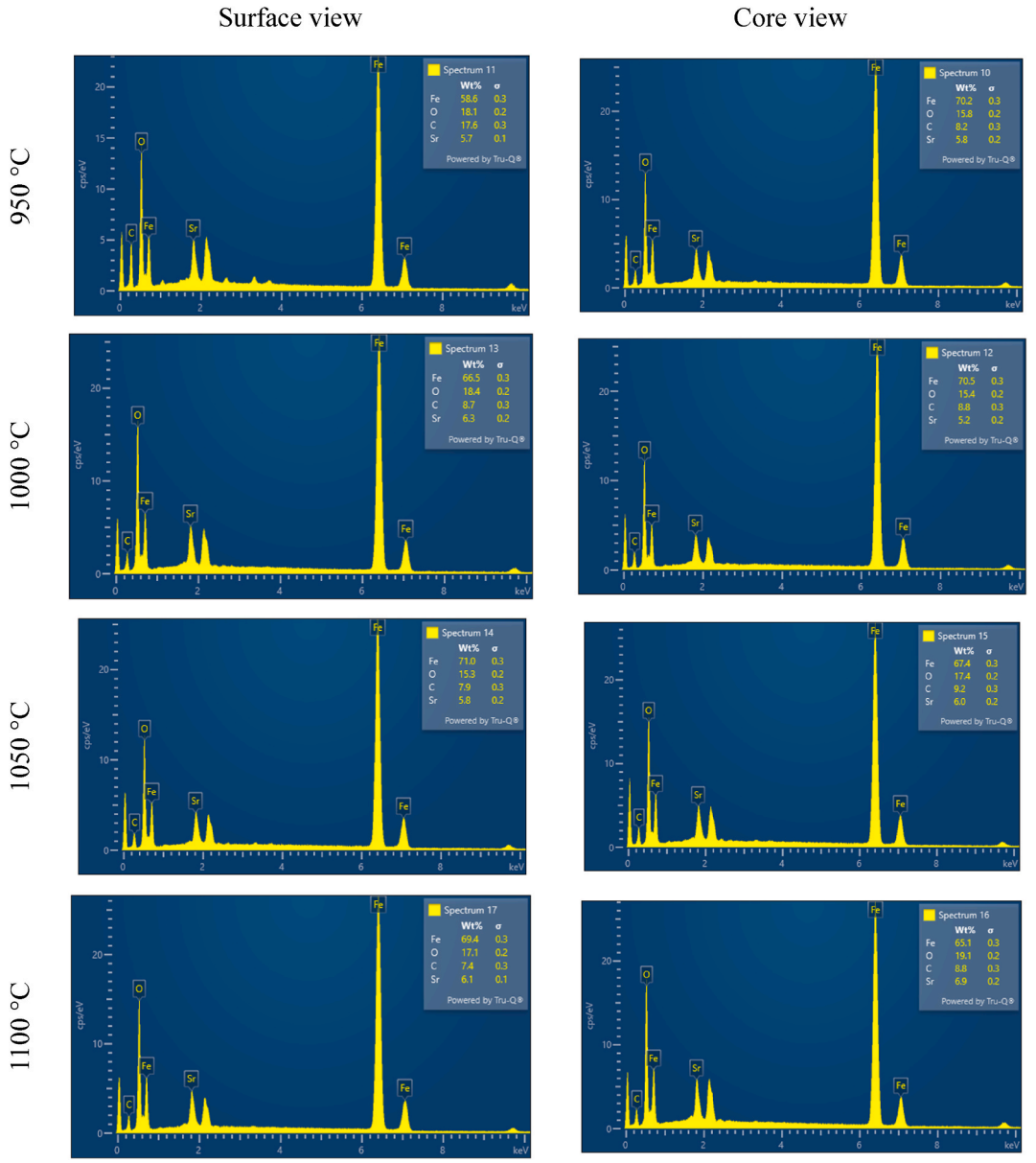

Fig. 5. EDX spectra of elemental distribution of sintered strontium ferrite (SrFe12O19) at different temperatures 950 °C, 1000 °C, 1050 °C, 1100 °C, in rows and from surface to core view in columns.

optimal crystallization. As the sintering temperature increased to 1000 °C, the relative density improved to 89.76 %, reaching an optimum density of 91.44 % at 1050 °C. However, a subsequent increase to 1100 °C led to a decline in both density (4.6246 g/cm^3) and relative density (89.28 %). This decrease was attributed to the coexistence of a secondary phase, α-Fe2O3, and potential multistage boundary melting during high-temperature sintering. X-ray diffraction (XRD) analysis confirmed the magnetoplumbite structure ($P6_3/mmc$) in all samples, with the presence of α-Fe2O3 observed at 1100 °C. The crystallinity and intensity of peaks were notably higher in samples sintered at 1050 °C, contributing to their denser structure and recording higher TC values indicating direction along easy magnetization c-axis compared to samples sintered at other temperatures. Moreover, sample sintered at 1050 °C revealed the highest average crystalline size of 63.212 nm and positive macrostrain confirming it grain growth and better microstructure. Scanning electron microscopy (SEM) revealed that grain growth and crystallization increased with higher sintering temperatures, resulting in larger, well-defined grains. Elemental distribution analysis through energy-dispersive X-ray spectroscopy (EDX) indicated homogenous distribution of iron (Fe), strontium (Sr) and oxygen (O) elements, with variations in carbon distribution observed between surface and core regions. The magnetic properties showed temperature-dependent trends, with optimal values recorded at 1000 °C and 1050 °C for magnetization remanence (Mr), saturation magnetization (Ms), coercivity, and maximum energy product (BH)max. The squareness

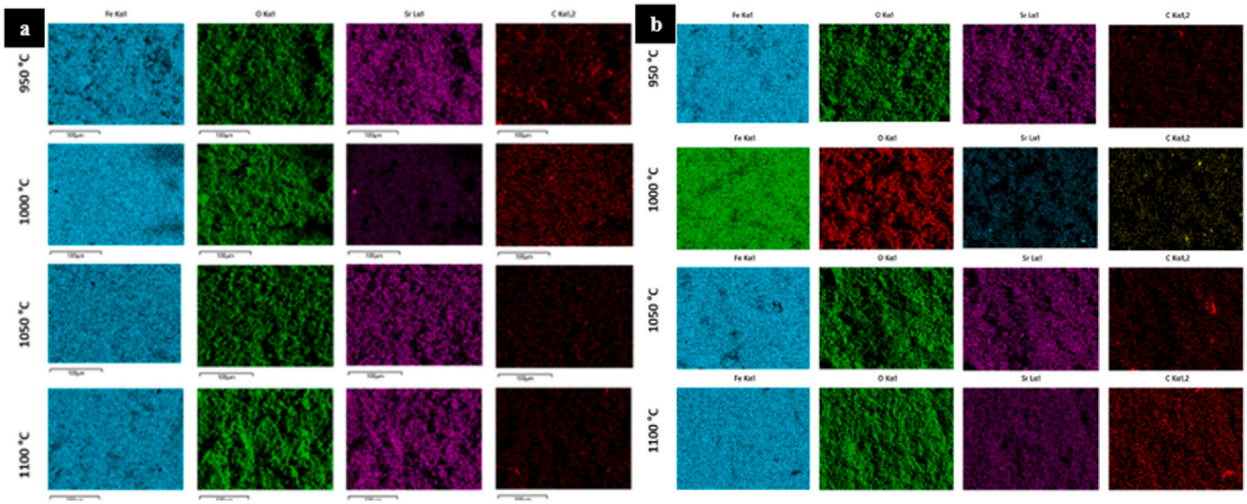

Fig. 6. Mapping of the sintered strontium hexaferrite (SrFe12O19) at different temperatures, (a) surface view, (b) core view of Fe, O, Sr, and C elements respectively.

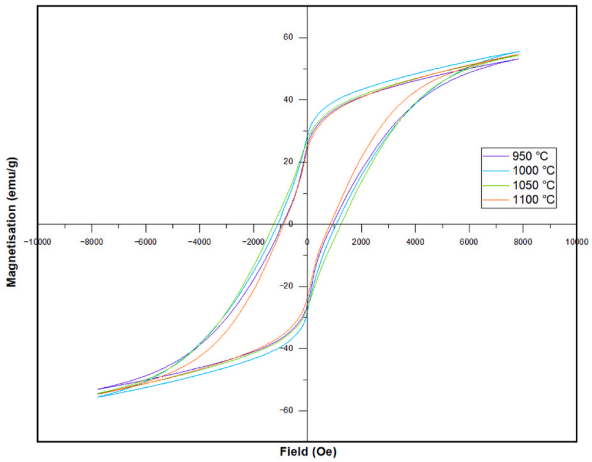

Fig. 7. Magnetic hysteresis loops of sintered SrM at different temperatures.

Table 5
Magnetic properties of strontium ferrite sintered at different temperatures.

Sample	Ms (emu/g)	Mr (emu/g)	Mr/Ms	Hc (Oe)	(BH) max (emu.Oe/g)
950 °C	53.187	25.684	0.483	928.11	23837.57
1000 °C	55.622	28.188	0.507	1082.2	30505.05
1050 °C	54.451	27.211	0.5	1252.0	34068.17
1100 °C	54.719	23.691	0.433	858.28	20333.51

ratio (Mr/Ms) of more than 0.4 indicated a dominance of Stoner-Wohlfarth behaviour in the studied samples. In summary, the sintering temperature significantly influences the microstructure, crystallinity, and magnetic properties of strontium hexaferrite, with an optimum condition observed at 1050 °C, providing significant insights for potential applications in magnetic devices and adding new outcomes in M-type hexaferrite microwave sintering studies. Further exploration of crystal structure and morphology is recommended for a comprehensive understanding of the material's behavior at higher sintering temperatures.

Data availability statement

Data will be made available on request.

Table 6
Comparison of sintering temperature, sintering method, and magnetic properties obtained from literature.

No	Sintering Temperature (°C)	Sintering method	Coercivity Hc (Oe)	Mr (emu/g)	Ms (emu/g)	Ref
1	1200	Conventional	3662	36	70	[57]
2	1140	Microwave	3343	36.182	70.322	[52]
3	1100	Cold	1500	–	49.2	[28]
4	1100	Cold	2800	–	68	[46]
5	600	Conventional	196.7	3.7	14.6	[51]
6	840	microwave	623.8	–	53.6	[37]
7	900	conventional	1039	–	40	[37]
8	1150	Microwave + Sol-gel	5594.53	33	50.43	[33]
9	1000–1050	Microwave	1252	28.188	55.622	Current study

CRediT authorship contribution statement

Wail M. Matran: Writing – original draft, Methodology, Investigation, Software, Data curation. **Mazli Mustapha:** Writing – review & editing, Supervision, Resources, Methodology, Funding acquisition. **Mohd Faizairi Nor:** Writing – review & editing, Validation. **Faizal Mustapha:** Resources, Formal analysis. **Fahd Saeed Alakbari:** Writing – review & editing, Validation, Visualization, Methodology, Conceptualization. **Gamal Al-shawesh:** Writing – review & editing, Validation. **Mohammed Bawahab:** Writing – review & editing, Validation.

Declaration of competing interest

The authors declare that they have no known competing financial interests or personal relationships that could have appeared to influence the work reported in this paper.

Acknowledgements

The authors are grateful and acknowledge the financial support provided by The Ministry of Higher Education-Malaysia (MOHE) under the Fundamental Research Grant (FRGS-Grant No. FRGS/1/2021/TK0/UTP/02/19). The authors would like to thank Universiti Teknologi PETRONAS for providing the resources to perform this research.

References

[1] J. Ormerod, Permanent magnet markets and applications, in: Modern Permanent Magnets, Elsevier, 2022, pp. 403–434.
[2] R.C. Pullar, Hexagonal ferrites: a review of the synthesis, properties and applications of hexaferrite ceramics, Prog. Mater. Sci. 57 (2012) 1191–1334.
[3] C. Granados-Miralles, M. Saura-Múzquiz, H.L. Andersen, Permanent Magnets Based on Hard Ferrite Ceramics, 2023.
[4] C. Granados-Miralles, P. Jenuš, On the potential of hard ferrite ceramics for permanent magnet technology—a review on sintering strategies, J. Phys. D Appl. Phys. 54 (2021) 303001.
[5] A. Leader, G. Gaustad, C. Babbitt, The effect of critical material prices on the competitiveness of clean energy technologies, Mater Renew Sustain Energy 8 (2019) 8.
[6] Y. Yang, A. Walton, R. Sheridan, K. Güth, R. Gauß, O. Gutfleisch, M. Buchert, B.-M. Steenari, T. Van Gerven, P.T. Jones, REE recovery from end-of-life NdFeB permanent magnet scrap: a critical review, Journal of Sustainable Metallurgy 3 (2017) 122–149.
[7] S. Mahmood, I. Bsoul, Tuning the magnetic properties of M-type hexaferrites, ArXiv Preprint ArXiv:1707.07243 1 (2017) 1–47.
[8] R.B. Jotania, S.H. Mahmood, Magnetic Oxides and Composites, Materials Research Forum LLC, 2018.
[9] D.V. Singh, R. Jasrotia, R. Kumar, P. Raizada, S. Thakur, K. Batoo, M. Singh, A current review on the synthesis and magnetic properties of M-type hexaferrites material, World J. Condens. Matter Phys. 8 (2018) 36–61, https://doi.org/10.4236/wjcmp.2018.82004.
[10] E.A. Nesbitt, R.D. Heidenreich, Magnetic annealing in perminvar. II. Magnetic properties, J. Appl. Phys. 30 (1959) 1000–1003.
[11] J. Du, T. Zhou, L. Lian, Y. Liu, Y. Du, Two-step sintering of M-type strontium ferrite with high coercivity, Ceram. Int. 45 (2019) 6978–6984, https://doi.org/10.1016/j.ceramint.2018.12.197.
[12] R. Jasrotia, J. Prakash, R. Verma, P. Thakur, A. Kandwal, F. Wan, A. Thakur, Synthesis, characterization, and applications of doped barium hexaferrites: a review, Phys. B Condens. Matter (2023) 415202.
[13] J.F. Wang, C.B. Ponton, R. Grössinger, I.R. Harris, A study of La-substituted strontium hexaferrite by hydrothermal synthesis, J. Alloys Compd. 369 (2004) 170–177, https://doi.org/10.1016/j.jallcom.2003.09.097.
[14] F. Haberey, A. Kockel, The formation of strontium hexaferrite SrFe 12 O 19 from pure iron oxide and strontium carbonate, IEEE Trans. Magn. 12 (1976) 983–985.
[15] G. Asti, M. Carbucicchio, A. Deriu, E. Lucchini, G. Slokar, Magnetic characterization of Ca substituted Ba and Sr hexaferrites, J. Magn. Magn Mater. 20 (1980) 44–46, https://doi.org/10.1016/0304-8853(80)90523-5.
[16] S.B. Dhuban, S. Ramesh, C.Y. Tan, Y.H. Wong, U.J. Alengaram, W.D. Teng, F. Tarlochan, U. Sutharsini, Sintering behaviour and properties of manganese-doped alumina, Ceram. Int. 45 (2019) 7049–7054.
[17] D. Agrawal, Microwave sintering of ceramics, composites and metallic materials, and melting of glasses, Trans. Indian Ceram. Soc. 65 (2006) 129–144.
[18] H. Sözeri, Z. Mehmedi, H. Kavas, A. Baykal, Magnetic and microwave properties of BaFe12O19 substituted with magnetic, non-magnetic and dielectric ions, Ceram. Int. 41 (2015) 9602–9609, https://doi.org/10.1016/j.ceramint.2015.04.022.
[19] M.A. Almessiere, Y. Slimani, B. Unal, T.I. Zubar, A. Sadaqat, A. V Trukhanov, A. Baykal, Microstructure, dielectric and microwave features of [Ni0. 4Cu0. 2Zn0. 4](Fe2− xTbx) O4 (x≤ 0.1) nanospinel ferrites, J. Mater. Res. Technol. 9 (2020) 10608–10623.
[20] M. Oghbaei, O. Mirzaee, Microwave versus conventional sintering: a review of fundamentals, advantages and applications, J. Alloys Compd. 494 (2010) 175–189.
[21] Y. V Bykov, S. V Egorov, A.G. Eremeev, V. V Kholoptsev, I. V Plotnikov, K.I. Rybakov, V.E. Semenov, A.A. Sorokin, Effects of microwave heating in nanostructured ceramic materials, Powder Metall. Met Ceram. 49 (2010) 31–41.

[22] S. Das, T.R. Curlee, Microwave sintering of ceramics-can we save energy, Am. Ceram. Soc. Bull. 66 (1987) 1093–1094.
[23] Z.Y. Chen, Y. Zhou, F. Chen, Z.K. Feng, Influence of microwave calcination on microstructure and magnetic properties of Sr-hexagonal ferrite, in: Adv Mat Res, Trans Tech Publ, 2013, pp. 741–744.
[24] J.G.P. Binner, I. Caro, J. Firkins, Microwave sintering of nanometer and micrometer ferrite powders, J. Microw. Power Electromagn. Energy 34 (1999) 131–136.
[25] G. Obara, H. Yamamoto, M. Tani, M. Tokita, Magnetic properties of spark plasma sintering magnets using fine powders prepared by mechanical compounding method, J. Magn. Magn Mater. 239 (2002) 464–467.
[26] Z.A. Munir, U. Anselmi-Tamburini, M. Ohyanagi, The effect of electric field and pressure on the synthesis and consolidation of materials: a review of the spark plasma sintering method, J. Mater. Sci. 41 (2006) 763–777.
[27] H.G. Mohammed, T.M.B. Albarody, S. Susilawati, S. Gohari, A. Doyan, S. Prayogi, M.R. Bilad, R. Alebrahim, A.A.H. Saeed, Process Optimization of in situ magnetic-anisotropy spark plasma sintering of M-type-based barium hexaferrite BaFe12O19, Materials 14 (2021) 2650.
[28] A. Serrano, E. Garcia-Martin, C. Granados-Miralles, J. Lopez-Sanchez, G. Gorni, A. Quesada, J.F. Fernandez, Effect of organic solvent on the cold sintering processing of SrFe12O19 platelet-based permanent magnets, J. Eur. Ceram. Soc. 42 (2022) 1014–1022.
[29] M. Biesuz, G. Taveri, A.I. Duff, E. Olevsky, D. Zhu, C. Hu, S. Grasso, A theoretical analysis of cold sintering, Adv. Appl. Ceram. 119 (2020) 75–89.
[30] J. Guo, S.S. Berbano, H. Guo, A.L. Baker, M.T. Lanagan, C.A. Randall, Cold sintering process of composites: bridging the processing temperature gap of ceramic and polymer materials, Adv. Funct. Mater. 26 (2016) 7115–7121.
[31] V.G. Karayannis, Microwave sintering of ceramic materials, in: IOP Conf Ser Mater Sci Eng, IOP Publishing, 2016 012068.
[32] J.D. Katz, Microwave sintering of ceramics, Annu. Rev. Mater. Sci. 22 (1992) 153–170.
[33] S. Kanagesan, S. Jesurani, R. Velmurugan, S. Prabu, T. Kalaivani, Study of morphological and magnetic properties of microwave sintered barium strontium hexaferrite, J. Mater. Sci. Mater. Electron. 23 (2012) 1511–1514, https://doi.org/10.1007/s10854-012-0620-1.
[34] S. Moratal, R. Benavente, M.D. Salvador, F.L. Peñaranda-Foix, R. Moreno, A. Borrell, Microwave sintering study of strontium-doped lanthanum manganite in a single-mode microwave with electric and magnetic field at 2.45 GHz, J. Eur. Ceram. Soc. 42 (2022) 5624–5630.
[35] K. Abduraoof, R. Balaji, S. Jayakumar, G.M. Joshi, Abnormal grain growth free strontium barium niobate by microwave assisted sintering, Ferroelectrics 481 (2015) 196–205.
[36] Y. Qinghui, Z. Huaiwu, L. Yingli, W. Qiye, J. Lijun, Microstructure and magnetic properties of microwave sintered NiCuZn ferrite for application in LTCC devices, Mater. Lett. 79 (2012) 103–105.
[37] Q. Yang, H. Zhang, Y. Liu, Q. Wen, Microstructure and magnetic properties of microwave sintered M-type barium ferrite for application in LTCC devices, Mater. Lett. 63 (2009) 406–408.
[38] U. Sutharsini, S. Ramesh, Y.H. Wong, H. Misran, F. Yusuf, C.Y. Tan, J. Purbolaksono, W.D. Teng, Effect of sintering holding time on low-temperature degradation of yttria stabilised zirconia ceramics, Mater. Res. Innovat. 18 (2014) S6–S408.
[39] M.L. Rahman, S. Rahman, B. Biswas, M.F. Ahmed, M. Rahman, N. Sharmin, Investigation of structural, morphological and magnetic properties of nanostructured strontium hexaferrite through co-precipitation technique: impacts of annealing temperature and Fe/Sr ratio, Helliyon 9 (2023).
[40] Y. Kim, Y.-K. Hong, S.J. Park, Spark plasma sintering behaviors of M-type barium hexaferrite nano powders, Journal of Powder Materials 21 (2014) 256–259.
[41] K. Kang, J. Byun, M. Jeen, G. Jo, Y.-K. Baek, J. Lee, H. Jeen, Effect of sintering time on electronic properties of strontium hexaferrite, Ceram. Int. 48 (2022) 12476–12482.
[42] V. Bilovol, M. Sikora, R.M. García, K. Berent, M. Gajewska, A. Szkudlarek, SrFe12O19/CoFe2O4 magnetic composites: nanoparticle size and effect of annealing temperature on magnetic properties, J. Magn. Magn Mater. 563 (2022) 169987.
[43] R. Sun, X. Li, A. Xia, S. Su, C. Jin, Hexagonal SrFe12O19 ferrite with high saturation magnetization, Ceram. Int. 44 (2018) 13551–13555.
[44] V. Bilovol, M. Sikora, R.M. García, K. Berent, M. Gajewska, A. Szkudlarek, SrFe12O19/CoFe2O4 magnetic composites: nanoparticle size and effect of annealing temperature on magnetic properties, J. Magn. Magn Mater. 563 (2022) 169987.
[45] Y. Kaneko, K. Kitajima, N. Takusagawa, Effects of CaO and SiO2 addition on microstructure and intrinsic coercivity of sintered Sr-ferrite, J. Ceram. Soc. Jpn. 100 (1992) 1435–1439.
[46] E. García-Martín, C. Granados-Miralles, S. Ruiz-Gómez, L. Pérez, A. del Campo, J.C. Guzmán-Mínguez, C. de Julián Fernández, A. Quesada, J.F. Fernández, A. Serrano, Dense strontium hexaferrite-based permanent magnet composites assisted by cold sintering process, J. Alloys Compd. 917 (2022) 165531.
[47] J. Muller, A. Collomb, A new representation of the bipyramidal site in the SrFe12O19 M-type hexagonal ferrite between 4.6 and 295 K, J. Magn. Magn Mater. 103 (1992) 194–203.
[48] M. Zhang, J. Dai, Q. Liu, Q. Li, Z. Zi, Fabrication and magnetic properties of hexagonal BaFe12O19 ferrite obtained by magnetic-field-assisted hydrothermal process, Curr. Appl. Phys. 18 (2018) 1426–1430.
[49] R.R. Prabhu, M. Abdul Khadar, Study of optical phonon modes of CdS nanoparticles using Raman spectroscopy, Bull. Mater. Sci. 31 (2008) 511–515.
[50] Z.Y. Chen, Y. Zhou, F. Chen, Z.K. Feng, Influence of microwave calcination on microstructure and magnetic properties of Sr-hexagonal ferrite, Adv. Mater. Res. 668 (2013) 741–744.
[51] K. Kang, J. Byun, M. Jeen, G. Jo, Y.-K. Baek, J. Lee, H. Jeen, Effect of sintering time on electronic properties of strontium hexaferrite, Ceram. Int. 48 (2022) 12476–12482.
[52] M. Jin, X. Wang, Z. Wang, H. Jiang, K. Liu, Effects of atmosphere on the microstructure and magnetic properties of strontium ferrites with microwave-assisted sintering, J Supercond Nov Magn 28 (2015) 3059–3063.
[53] M.R. Kumar, Z.J. Yu, Q. Pan, Large scale production of SrFe12O19 nanoparticles with low calcination temperature, Mater. Res. Express 4 (2017) 095007.
[54] K. Praveena, S. Katlakunta, H.S. Virk, Structural and magnetic properties of Mn-Zn ferrites synthesized by microwave-hydrothermal process, Solid State Phenom. 232 (2015) 45–64.
[55] E.C. Stoner, E.P. Wohlfarth, A mechanism of magnetic hysteresis in heterogeneous alloys, Phil. Trans. Roy. Soc. Lond. Math. Phys. Sci. 240 (1948) 599–642.
[56] W.M. Matran, M. Mustapha, M.F. Nor, The influences of additives in M− type (Ba and Sr) hexaferrites' microstructure, sintering and magnetic properties: a review, Mater Today Proc 96 (2024) 78–83.
[57] P. Sahu, S.N. Tripathy, R. Pattanayak, R. Muduli, N. Mohapatra, S. Panigrahi, Effect of grain size on electric transport and magnetic behavior of strontium hexaferrite (SrFe 12 O 19), Appl. Phys. A 123 (2017) 1–10.